Kinematic Corner Smoothing for High Speed Machine Tools

Article *in* International Journal of Machine Tools and Manufacture · June 2016

DOI: 10.1016/j.ijmachtools.2016.05.009

Shingo Tajima
Oregon State University

Burak Sencer
Oregon State University

International Journal of Machine Tools & Manufacture 108 (2016) 27–43

Contents lists available at ScienceDirect

International Journal of Machine Tools & Manufacture

journal homepage: www.elsevier.com/locate/ijmactool

Kinematic corner smoothing for high speed machine tools

Shingo Tajima, Burak Sencer*

Oregon State University, School of Engineering, Mechanical Engineering Department, Corvallis, OR, USA

ARTICLE INFO

Article history:
Received 7 April 2016
Received in revised form
28 May 2016
Accepted 31 May 2016
Available online 2 June 2016

Keywords:
Numerical control(NC)
Trajectory generation
Corner smoothing
Motion control

ABSTRACT

This paper presents a novel kinematic corner smoothing technique for high-speed CNC machine tools. Typically, reference tool-paths compromised of short G01 moves are geometrically smoothed by means of arcs and splines within the NC system. In this study, a continuous feed motion is generated by directly planning jerk limited velocity transitions for the drives in the vicinity of sharp corners of the tool-path. This approach completely eliminates the need for geometry based path smoothing and feed planning. Contouring errors at sharp corners are controlled analytically by accurately calculating cornering speed and duration. Since proposed approach bases on kinematically planning axis motion profiles, it exploits acceleration and jerk limits of the drives and delivers a near-time optimal motion. Experimental validation and comparisons are presented to show significant improvement in the cycle time and accuracy of contouring Cartesian tool-paths.

1. Introduction

CAD systems are utilized to design complex geometries based on smooth curves such as NURBS or B-splines [1]. Direct interpolation of these curves is proven to be superior in terms of providing smoother and faster motion in high-speed machining [2,3]. However, most CNC machines are not capable of efficiently interpolating higher order parametric curves in real-time. Accurate calculation of curve lengths [4], planning of time efficient feed profiles [5–7] suppression of feed fluctuations [8] and control of chord errors during real-time interpolation are major bottlenecks still being addressed both by academia and NC builders. Instead, CAM systems are aided to discretize original smooth part geometry with numerous short line segments, and NC systems are fed with linear "point-to-point" motion commands. Interpolating paths compromised of linear segments limits productivity. Since linear moves are not continuous, motion has to stop at junction points of linear segments, i.e. corners, leading elongated cycle times and generating rough, cornered surface finishes [9].

Local "corner blending (smoothing)" techniques have been proposed to achieve non-stop continuous motion [10,11]. The idea is well-known and straightforward. In order to realize a continuous transition between consecutive linear segments, sharp corner is replaced with a smooth blending curve by the NC system. As a result, the corner is no longer sharp, and reference path deviates from the original geometry. As a matter of fact, this deviation is not detrimental during high-speed machining since sharp corners are rarely executed in roughing or semi finishing operations. Instead, corners are programmed to be traversed continuously, subject to manufacturing tolerance constraints and kinematic limits of the machine [12]. Thus, key requirements in continuous cornering are continuity [9], accuracy [13] and speed [14].

Current literature solves corner smoothing problem in two steps, namely; curve fitting followed by feed profile planning. First, corner geometry is smoothed by fitting a highly continuous curve under user specified cornering tolerances. Jouaneh et. al. [10] replaced the corner with a circular arc for fast cornering. However, a circular arc only delivers velocity continuous (C^1) motion transition. Later they used two clothoid curves to realize acceleration continuous (C^2) motion transition[11]. Yutkowitz and Chester [15] utilized two quartic splines to generate curvature continuous cornering geometry within user-specified tolerances. Sencer et al. [16] solved curve fitting problem with a single Quintic Bezier curve and others [17–21] used B-spline curves to control both corner geometry and the continuity. Beudaert et. al. [22] extended sharp corner smoothing in five-axis machining paths.

Once sharp corners are smoothened, it becomes a mixture of linear segments continuously blended with splines. Thus, the second step is scheduling of a feed profile. Due to curved corner profile, tangential speed (feedrate) must be lowered so that axis velocity and acceleration limits are not violated at corner sections [9]. Jerk limited acceleration profile (JLAP) is widely used in high-speed machining [23,24]. It generates trapezoidal acceleration transitions with piecewise constant jerk segments, which helps avoiding excitement of inertial vibrations of feed drive system and provides a practical balance between smoothness and time-optimality. Erkorkmaz and Altintas [25] planned JLAP based trajectories along spline tool-paths. Others generated JLAP based feed profiles along corner smoothed tool-paths [16,20,19].

[*] Corresponding author.

http://dx.doi.org/10.1016/j.ijmachtools.2016.05.009
0890-6955/© 2016 Elsevier Ltd. All rights reserved.

Nevertheless, separation of corner smoothing problem into curve fitting and feed planning is an inefficient approach. Since smoothened corner geometry is essentially a parametric curve, it suffers from bottlenecks related to real-time interpolation [8,13,16]. In addition, planning of a time optimal feed profile along corner blend is computationally stringent[6]. As a result, conservative cornering speeds are selected in real-time implementation [9]. Recent approaches are towards development of kinematic corner blending techniques, which eliminate the need for parametric curve fitting. Okwudire and Ding [14] used optimal control to generate time-optimal cornering trajectories. Weck and Ye [26] and recently, Sencer et al. [27] investigated on filtering techniques to accurately travel along sharp corners. Tsai and Huang [28] investigated incorporation of servo dynamics into cornering trajectory generation to improve dynamic contouring accuracy.

This paper proposes a novel approach where continuous cornering is achieved without fitting a parametric curve. Instead, we solve the problem "kinematically" by smoothly blending axis velocities from one segment to the other based on the JLAP. Fastest cornering speed, which respects axis velocity, acceleration and jerk limits, and at the same time generates a cornering trajectory within user-specified cornering tolerance computed analytically. Since one of the axis kinematic limits is primarily saturated, proposed "kinematic corner blending" technique provides near time-optimal cornering motion. Section 2 presents the proposed kinematic corner smoothing method based on the JLAP. Section 3 shows illustrative examples, experimental validations and comparisons to past literature. Lastly, Section 4 provides conclusions and discussions.

2. Kinematic corner smoothing problem

Majority of NC tool-paths contain series of linear segments as shown in Fig. 1a. A single planar*(x,y)* cornering scenario encountered on a Cartesian manufacturing machine is shown in Fig. 1b. The two consecutive linear segments intersect each other to generate the sharp corner, $P_c = [x_c, y_c]$. The angles θ_1 and θ_2 define orientation of linear segments, and $\overrightarrow{t_s} = [\cos(\theta_1), \sin(\theta_1)]^T$ and $\overrightarrow{t_e} = [\cos(\theta_1 + \theta_2), \sin(\theta_1 + \theta_2)]^T$ are the unit vectors defining feed directions along them. As observed, the geometry is position (G^0) continuous, which allows continuous interpolation of axis position commands. However, the feed direction changes discontinuously from t_s to t_e at sharp corner point, P_c. As a result, if sharp corner is to be traveled at constant speed, infinite amount of acceleration is necessary to alter axis velocities at corner point, which saturates the drives. The machine simply has to come to a full-stop at the sharp corner before continuing to the consecutive linear segment. This approach severely elongates cycle time of a manufacturing operation. Therefore, current techniques focus on smoothening sharp corner geometry within specified cornering tolerance so that the machine could traverse non-stop along linear segmented tool-path.

This paper proposes a novel technique where instead of smoothing the path geometry, a smooth and controlled cornering trajectory is generated by designing motion profiles of the axes. Fig. 2 shows proposed smoothened sharp corner profile. The tool approaches vicinity of the corner at a cornering speed of V_c and an acceleration A_c. As shown in Fig. 2a–b, the idea is to smoothly blend axis kinematic motion profiles from entry and to the exit of corner so that feed direction can be changed continuously. In order to stay within kinematic limits of the drives, axis kinematic profiles are interpolated at a finite cornering duration of T_c, which in return introduces deviation from original path geometry. Selecting identical V_c and A_c at both ends of the corner generates a symmetrical corner profile around the bisector of the unit tangent vectors, and the maximum deviation from the original sharp cornered geometry occurs at the center (see Fig. 2a). The problem is to determine the maximum cornering velocity and accelerations, which keeps cornering trajectory within user specified cornering tolerance, ε and utilizes drive's acceleration A_{max} and jerk J_{max} limits to minimize total cornering cycle time.

2.1. Jerk limited acceleration profile

Jerk limited acceleration profile (JLAP) is a widely used trajectory generation scheme in modern CNC machine tools [9,23,30]. It is used to accelerate or decelerate the tool from an initial velocity and acceleration, to a final velocity and acceleration within pre-determined acceleration and jerk limits. Fig. 3 shows the jerk limited acceleration profile. It consists of 3 phases. In phase 1, acceleration is increased at constant rate controlled by the piecewise constant jerk, J_1. This is followed by a constant (cruise) acceleration phase A, and acceleration is decelerated at a constant rate of J_3 in phase 3. Through this 3-phased acceleration profile, both initial velocity of V_s and acceleration A_s are smoothly blended with the final velocity V_e and acceleration A_e. If the initial conditions for displacement S_s, velocity V_s and acceleration A_s are known, and the jerk profile is known, acceleration *a(t)*, velocity *v(t)* and displacement *s(t)* profiles can be obtained by integrating the jerk *j(t)* as,

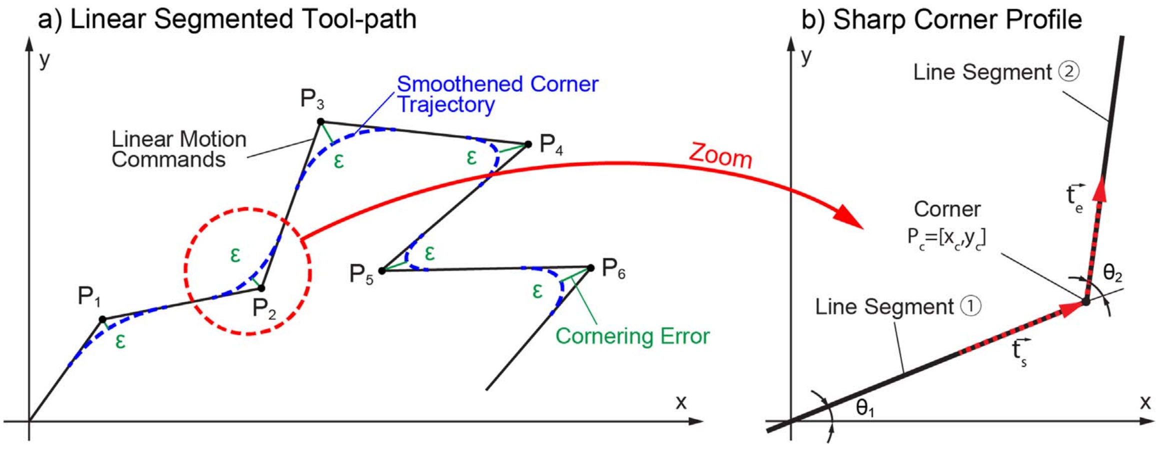

Fig. 1. Sharp corner smoothing of discrete tool-paths.

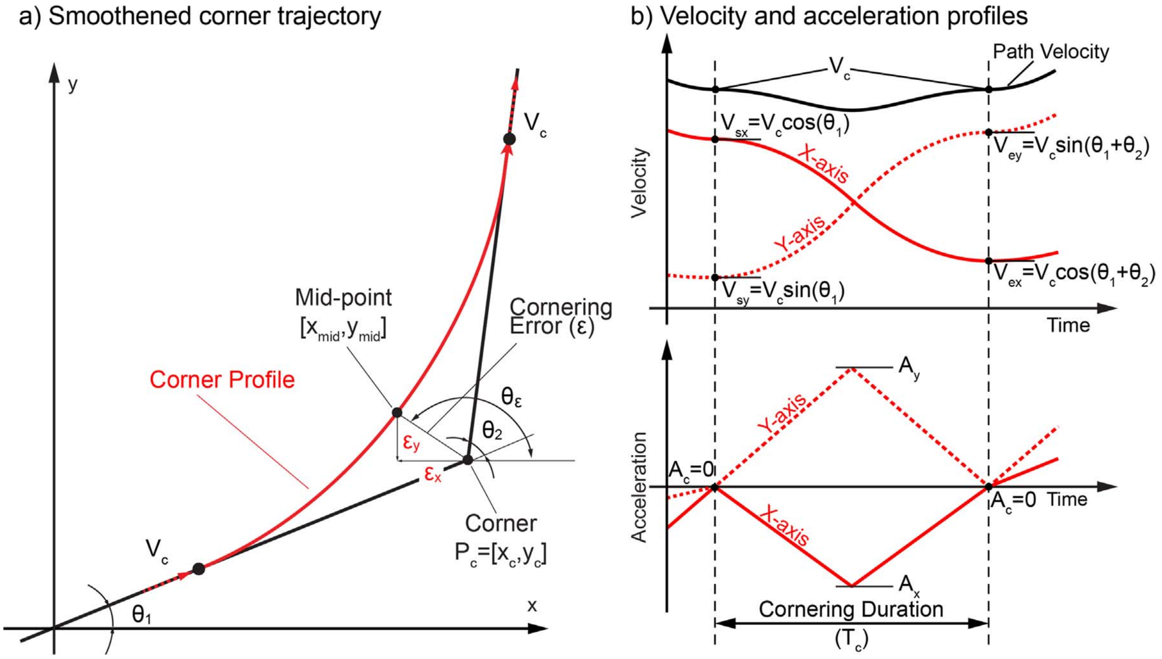

Fig. 2. Kinematic corner smoothing (KCS) strategy with interrupted acceleration.

$$a(t) = A_s + \int_0^t j(\tau)d\tau, \quad v(t) = V_s + \int_0^t a(\tau)d\tau, \quad s(t) = S_s + \int_0^t v(\tau)d\tau, \tag{1}$$

The jerk profile during acceleration/deceleration durations in Fig. 3 can be written as,

$$j(\tau) = \begin{cases} J_1,\ 0 \le t < t_1 \\ 0,\ t_1 \le t < t_2 \\ J_3,\ t_2 \le t < t_3 \end{cases} \tag{2}$$

where t denotes absolute time, t_1, t_2, t_3 denote the time boundaries of each phase; J_1 and J_3 are jerk values in phases 1 and 3. Integrating Eq. (2) with respect to time, reveals the trapezoidal acceleration profile

$$a(\tau) = \begin{cases} A_s + J_1\tau_1, & 0 \le t < t_1 \\ A, & t_1 \le t < t_2 \\ A + J_3\tau_3, & t_2 \le t \le t_3 \end{cases} \tag{3}$$

where A is the acceleration amplitude, and τ_k is the relative time parameter, which starts at the beginning of the kth phase as shown in Fig. 3. Similarly, integrating Eq. (3) with respect to time generates the velocity profile as,

$$v(\tau) = \begin{cases} V_s + A_s\tau_1 + \frac{1}{2}J_1\tau_1^2, & 0 \le t \le t_1 & V_1 = V_s + A_sT_1 + \frac{1}{2}J_1T_1^2 \\ V_1 + A\tau_2, & t_1 \le t \le t_2 & V_2 = V_1 + AT_2 \\ V_2 + A\tau_3 + \frac{1}{2}J_3\tau_3^2, & t_2 \le t \le t_3 & V_e = V_2 + AT_3 + \frac{1}{2}J_3T_3^2 \end{cases} \tag{4}$$

where V_s is the initial velocity, and V_e denotes the final velocity reached at the end of the motion. T_k *(k=1,2,3)* is the duration of the k^{th} phase, and V_k is the velocity reached at the end of each corresponding phase. Again, integrating Eq. (4) with respect to time yields the displacement profile,

$$s(\tau) = \begin{cases} S_s + V_s\tau_1 + \frac{1}{2}A_s\tau_1^2 + \frac{1}{6}J_1\tau_1^3, & 0 \le t \le t_1 & S_1 = V_sT_1 + \frac{1}{2}A_sT_1^2 + \frac{1}{6}J_1T_1^3 \\ S_1 + V_1\tau_2 + \frac{1}{2}A\tau_2^2, & t_1 \le t \le t_2 & S_2 = S_1 + V_1T_2 + \frac{1}{2}AT_2^2 \\ S_2 + V_2\tau_3 + \frac{1}{2}A\tau_3^2 + \frac{1}{6}J_3\tau_3^3, & t_2 \le t \le t_3 & S_e = S_2 + V_2T_3 + \frac{1}{2}AT_3^2 + \frac{1}{6}J_3T_3^3 \end{cases} \tag{5}$$

where s_k (k=1,2,3) is the displacement reached at the end of each k^{th} phase.

In most general usage, jerk limited acceleration profile can be employed to generate smooth velocity and acceleration transition between given kinematic boundaries, i.e. V_s, V_e and A_s, A_e. Owing to the nature of the trapezoidal shape of the profile, acceleration amplitude A can be expressed as:

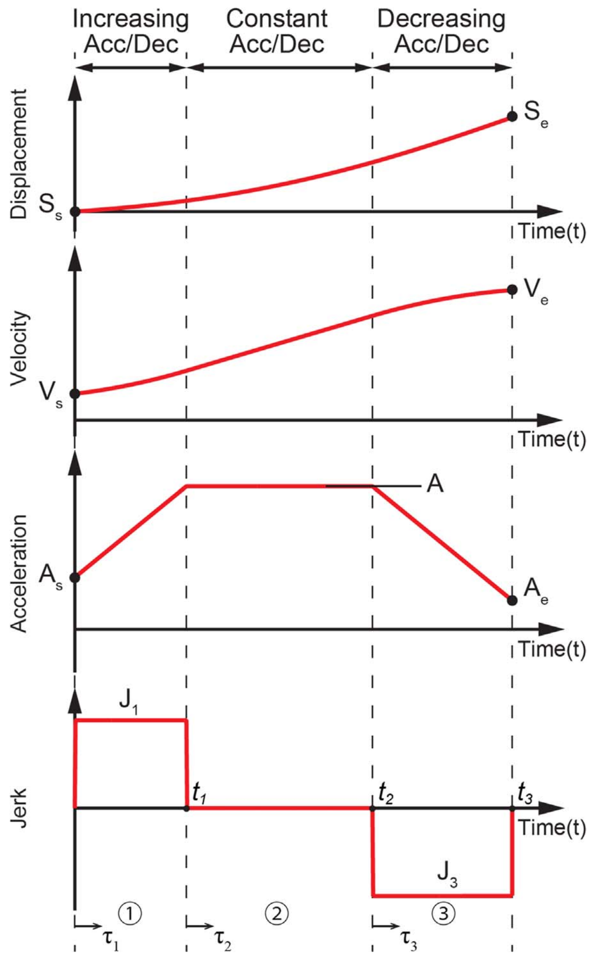

Fig. 3. Jerk limited acceleration profile (JLAP).

$$A = A_s + J_1 T_1 = A_e - J_3 T_3, \tag{6}$$

and correct signs for acceleration and jerk values can be determined from velocity and acceleration boundary conditions:

$$\begin{aligned} A &= \mathrm{sgn}(V_e - V_s)|A| \\ J_1 &= \mathrm{sgn}(A)|J_1| \\ J_3 &= -\mathrm{sgn}(A)|J_3|\} \end{aligned} \tag{7}$$

Note that a negative A indicates deceleration instead of acceleration in the motion. The signs of jerk amplitudes are modified accordingly. If the value of A is zero, this indicates absence of an acceleration phase.

The jerk limited acceleration profile is constructed by determining durations of all the three phases, T_1, T_2 and T_3. If a constant acceleration phase exists in the motion, maximum acceleration $A{=}A_{max}$ is reached at the end of phase 1. The maximum allowable jerk, J_{max} is used to minimize the total motion duration. Therefore, durations for phases 1 and 3 can be computed from Eq. (6) as:

$$T_1 = \frac{|A_{\max} - A_s|}{J_{\max}}, \quad T_3 = \frac{|A_{\max} - A_e|}{J_{\max}} \tag{8}$$

Knowing that both V_e and A_e are reached at the end of velocity transition, T_2 is computed from Eq. (4) to be:

$$T_2 = \frac{1}{A_{\max}}\left[|V_e - V_s| - \frac{A_{\max} + A_s}{2}T_1 - \frac{A_{\max} + A_e}{2}T_3\right] = \frac{1}{A_{\max}}\left[|V_e - V_s| - \frac{{A_{\max}}^2}{J_{\max}} + \frac{{A_s}^2 + {A_e}^2}{2J_{\max}}\right]. \tag{9}$$

On the other hand, if the velocity transition ΔV is small, and acceleration capacity of the drives is large, T_2 computed from Eq. (9) may yield a negative value, $T_2 < 0$. In this case, $T_2 = 0$ is set, which eliminates any constant acceleration phase, and acceleration amplitude is adjusted from Eq. (9):

$$A = \mathrm{sgn}(V_e - V_s)\sqrt{J_{\max}\,(V_e - V_s) + \frac{{A_s}^2 + {A_e}^2}{2}} \tag{10}$$

The non-zero jerk durations are then updated accordingly,

$$T_1 = \frac{|A - A_s|}{J_{\max}}, \quad T_3 = \frac{|A - A_e|}{J_{\max}} \tag{11}$$

Once all the segment durations are obtained from Eqs. (8), (9) and (11), jerk limited acceleration profile can be constructed to realize smooth velocity and acceleration transitions. The total distance traveled during the transition is obtained as:

$$L = \begin{cases} V_s\left(T_1 + T_2 + T_3\right) + \dfrac{1}{2}A_s T_1^2 + A_s T_1\left(T_2 + T_3\right) + \dfrac{1}{2}A\left(T_2 + T_3\right)^2 + \dfrac{1}{6}J_{\max}\left(T_1^3 - T_3^3\right) + \dfrac{1}{2}J_{\max} T_1^2\left(T_2 + T_3\right) & \text{if } T_2 \neq 0 \\ V_s\left(T_1 + T_3\right) + \dfrac{1}{2}A_s\left(T_1 + T_3\right) + \dfrac{1}{6}J_{\max}\left(T_1^3 - T_3^3\right) + \dfrac{1}{2}J_{\max} T_1 T_3\left(T_1 + T_3\right) & \text{if } T_2 = 0 \end{cases} \tag{12}$$

Please note that, although the most general form of the JLAP is given in above equations, typically the profile is used to generate smooth speed transition between two cruise velocities. In other words, initial and final accelerations are generally zero, $A_s = A_e = 0$, and construction of the profile becomes simpler. For instance, the acceleration profile becomes symmetrical from Eq. (3),

$$A = J_1 T_1 = J_3 T_3 \text{ where} \begin{cases} A = \operatorname{sgn}\left(V_e - V_s\right)|A| \\ J_1 = \operatorname{sgn}(A)|J| \text{ and } J_3 = -J \end{cases} \tag{13}$$

and durations of phases 1 and 3 can be become:

$$T_1 = T_3 = \frac{A_{\max}}{J_{\max}}. \tag{14}$$

Knowing that only V_e is reached at the end of velocity transition, T_2 can be computed from Eq. (4) to be

$$T_2 = \frac{|V_e - V_s|}{A_{\max}} - \frac{A_{\max}}{J_{\max}} \tag{15}$$

and the non-existence of constant acceleration phase, $T_2 < 0$, is handled by setting $T_2 = 0$ and acceleration amplitude is calculated as:

$$A = \operatorname{sgn}(V_e - V_s)\sqrt{J_{\max}|V_e - V_s|}, \tag{16}$$

and constant jerk durations are adjusted accordingly from Eq. (14):

$$T_1 = T_3 = \frac{|A|}{J_{\max}}. \tag{17}$$

Finally, total distance traveled during a velocity transition yields

$$L = \begin{cases} \dfrac{\left(V_e + V_s\right)\left(A_{\max}^2 + J_{\max} V_e - J_{\max} V_s\right)}{2A_{\max} J_{\max}} & \text{if } T_2 \neq 0 \\ \dfrac{\sqrt{\left(V_e + V_s\right)\left(J_{\max}\left(V_e - V_s\right)\right)}}{J_{\max}}, & \text{if } T_2 = 0 \end{cases} \tag{18}$$

The acceleration phase of the JLAP is presented above, and it can be constructed to either interpolate constant velocity transitions, or velocity transitions with initial accelerations. The deceleration phase can be planned by replacing acceleration amplitudes with negative deceleration values. Therefore, it is omitted here. Following sections present the proposed kinematic corner smoothing (KCS) algorithm designed based on the jerk limited acceleration profile.

2.2. *Kinematic corner smoothing (KCS) with interrupted acceleration*

This section presents the proposed kinematic corner smoothing (KCS) scheme applied to corners formed by the intersection of long straight lines. For such long line segments, smoothing is highly localized to a corner region that is typically a small fraction of the total length of the line. Thus, we assume that corners do not overlap each other, programmed feedrate along linear segments can be reached, and the machine has capacity to decelerate to a specified cornering speed, V_c Here, we assume that the cornering motion starts from a constant cornering speed V_c with zero initial acceleration $A_c = 0$. Therefore, we call this method "KCS with interrupted acceleration". As shown in Fig. 2b, V_c controls axis velocity boundary conditions at the start (V_{sx}, in V_{sy}) and end (V_{ex}, in V_{ey}) of a cornering trajectory. The objective is to determine the fastest cornering speed, V_c feasible so that axis velocity transitions can be planned, and resultant cornering trajectory deviates from original sharp corner profile by a predetermined geometric tolerance value, ε (See Fig. 2a).

Assuming that the cornering motion starts and ends at identical tangential cornering velocity V_c, individual x–y axis velocity profiles are planned based on the JLAP from Eq. (4) as:

$$v_x(\tau) = \left\{ \begin{array}{lll} V_{sx} + \frac{1}{2}J_{1x}\tau_1^2, & 0 \le t < t_1, & V_{1x} = V_{sx} + \frac{1}{2}J_{1x}T_1^2 \\ V_{1x} + A_x\tau_2, & t_1 \le t < t_2, & V_{2x} = V_{1x} + A_xT_2 \\ V_{2x} + A_x\tau_3 + \frac{1}{2}J_{3x}\tau_3^2, & t_2 \le t \le t_3, & V_{ex} = V_{2x} + A_xT_3 + \frac{1}{2}J_{3x}T_3^2 \end{array} \right\},$$

$$v_y(\tau) = \left\{ \begin{array}{lll} V_{sy} + \frac{1}{2}J_{1y}\tau_1^2, & 0 \le t < t_1, & V_{1y} = V_{sy} + \frac{1}{2}J_{1y}T_1^2 \\ V_{1y} + A_y\tau_2, & t_1 \le t < t_2, & V_{2y} = V_{1y} + A_yT_2 \\ V_{2y} + A_y\tau_3 + \frac{1}{2}J_{3y}\tau_3^2, & t_2 \le t \le t_3, & V_{ey} = V_{2y} + A_yT_3 + \frac{1}{2}J_{3y}T_3^2 \end{array} \right\} \quad (19)$$

where starting and ending velocity boundary conditions are calculated form Eq. (19) and corner geometry(See Fig. 3):

$$\underbrace{\left\{ \begin{array}{l} V_{sx} = V_c \cos(\theta_1) \\ V_{sy} = V_c \sin(\theta_1) \end{array} \right\}}_{\text{Starting Velocity Constraints}}, \underbrace{\left\{ \begin{array}{l} V_{ex} = V_c \cos(\theta_1 + \theta_2) = V_{sx} + A_x(T_2 + T_3) + 1/2J_{1x}T_1^2 + 1/2J_{3x}T_3^2 \\ V_{ey} = V_c \sin(\theta_1 + \theta_2) = V_{sy} + A_y(T_2 + T_3) + 1/2J_{1y}T_1^2 + 1/2J_{3y}T_3^2 \end{array} \right\}}_{\text{Ending Velocity Constraints}} \quad (20)$$

where $J_{1x}=-J_{3x}, J_{1y}=-J_{3y}$ are axis jerk, and A_x, A_y are axis cornering acceleration amplitudes. For a Cartesian motion system, identical jerk and acceleration limits are generally selected, i.e. $J_{max}=J_{xmax}=J_{ymax}$ and $A_{max}=A_{xmax}=A_{ymax}$. The total velocity transition for each axis during a cornering trajectory can be obtained from Eq. (20),

$$\left. \begin{array}{l} \Delta V_x = V_c\left|\cos(\theta_1 + \theta_2) - \cos(\theta_1)\right| \\ \Delta V_y = V_c\left|\sin(\theta_1 + \theta_2) - \sin(\theta_1)\right| \end{array} \right\} \quad (21)$$

Next, displacement boundary conditions are imposed to control the smoothened corner geometry. Since tangential velocity and acceleration are identical at start and end of the motion, cornering trajectory is symmetrical around the bisector of the unit tangent vectors, t_s t_e, and hence maximum geometrical deviation from the sharp corner point occurs in the middle of the cornering trajectory. Cartesian coordinates of the mid-point can be computed by integrating Eq. (19) and evaluating it at $t = T_1 + 1/2T_2$ as:

$$\left. \begin{array}{l} x_{mid} = V_c \cos(\theta_1)\left(T_1 + \frac{T_2}{2}\right) + \frac{1}{2}A_x\left(\frac{T_2}{2}\right)^2 + \frac{1}{6}J_{1x}T_1^3 + \frac{1}{2}J_{1x}T_1^2\left(\frac{T_2}{2}\right) \\ y_{mid} = V_c \sin(\theta_1)\left(T_1 + \frac{T_2}{2}\right) + \frac{1}{2}A_y\left(\frac{T_2}{2}\right)^2 + \frac{1}{6}J_{1y}T_1^3 + \frac{1}{2}J_{1y}T_1^2\left(\frac{T_2}{2}\right) \end{array} \right\}. \quad (22)$$

The original sharp corner location $P_c=[x_c, y_c]$ is considered relative from the start of the cornering motion, and it can be defined from the cornering geometry (see Fig. 2a) as:

$$\left. \begin{array}{l} x_c = L_c \cos(\theta_1) \\ y_c = L_c \sin(\theta_1) \end{array} \right\} \quad (23)$$

where L_c is the Euclidian length used for corner smoothing. L_c can be calculated based on the corner geometry and total displacement traveled by the drives. For instance, considering X-axis's motion, L_c can be obtained from Eq. (18) with the boundary velocity conditions given in Eq. (20) as:

$$\begin{array}{l} L_c\left(\cos(\theta_1) + \cos(\theta_1 + \theta_2)\right) = V_c \cos(\theta_1)T_1 + \frac{1}{6}J_{1x}T_1^3 + \left(V_c \cos(\theta_1) + \frac{1}{2}J_{1x}T_1^2\right)T_2 + \frac{1}{2}A_xT_2^2 \\ \qquad + \left(V_c \cos(\theta_1) + \frac{1}{2}J_{1x}T_1^2 + A_xT_2\right)T_3 + \frac{1}{2}A_xT_3^2 + \frac{1}{6}J_{3x}T_3^3 \end{array} \quad (24)$$

and the displacement constraints for the cornering motion is imposed from Eqs. (22)–(24):

$$\left. \begin{array}{l} \varepsilon_x = x_{mid} - x_c = V_c \cos(\theta_1)\left(T_1 + \frac{T_2}{2}\right) + \frac{1}{2}A_x\left(\frac{T_2}{2}\right)^2 + \frac{1}{6}J_{1x}T_1^3 + \frac{1}{2}J_{1x}T_1^2\left(\frac{T_2}{2}\right) - V_c \cos(\theta_1)\left(T_1 + \frac{T_2}{2}\right) \\ \varepsilon_y = y_{mid} - y_c = V_c \sin(\theta_1)\left(T_1 + \frac{T_2}{2}\right) + \frac{1}{2}A_x\left(\frac{T_2}{2}\right)^2 + \frac{1}{6}J_{1x}T_1^3 + \frac{1}{2}J_{1x}T_1^2\left(\frac{T_2}{2}\right) - V_c \sin(\theta_1)\left(T_1 + \frac{T_2}{2}\right) \end{array} \right\} \quad (25)$$

where $\varepsilon_x = \varepsilon \cos(\theta_\varepsilon)$, $\varepsilon_y = \varepsilon \sin(\theta_\varepsilon)$ are Cartesian projections of cornering toleranceε, and $\theta_\varepsilon = \pi/2 + \theta_1 + \theta_2/2$ is the bisector of the corner (See Fig. 2a).

Maximum cornering velocity, V_c is sought to generate the fastest cornering speed, which saturates at least one of the axis acceleration or jerk limits. Therefore, V_c is constrained based on the axis, which experiences the largest velocity transition identified from Eq. (21). For instance, if $\Delta V_x > \Delta V_y$, X-axis becomes the "limiting axis". Velocity and displacement kinematic conditions are combined from Eqs. (20) and (25) for the x-axis as:

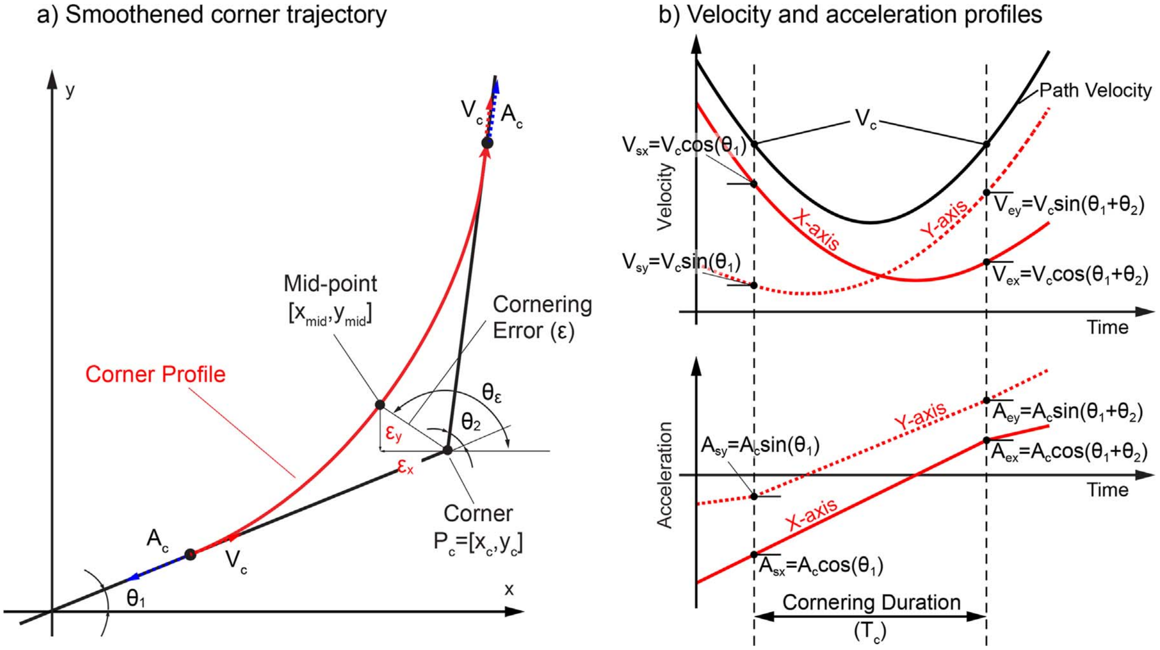
a) Smoothened corner trajectory
y
x
V_c
A_c
Mid-point
$[x_{mid}, y_{mid}]$
Cornering
Error (ε)
Corner Profile
θ_ε
θ_2
ε_y
ε_x
Corner
$P_c=[x_c, y_c]$
A_c
V_c
θ_1
b) Velocity and acceleration profiles
Velocity
V_c
Path Velocity
$V_{sx}=V_c\cos(\theta_1)$
X-axis
Y-axis
$V_{ey}=V_c\sin(\theta_1+\theta_2)$
$V_{sy}=V_c\sin(\theta_1)$
$V_{ex}=V_c\cos(\theta_1+\theta_2)$
Time
Acceleration
Y-axis
$A_{ey}=A_c\sin(\theta_1+\theta_2)$
$A_{sy}=A_c\sin(\theta_1)$
$A_{ex}=A_c\cos(\theta_1+\theta_2)$
Time
X-axis
$A_{sx}=A_c\cos(\theta_1)$
Cornering Duration
(T_c)

Fig. 4. Kinematic Corner smoothing with uninterrupted acceleration.

$$\left.\begin{aligned}&\text{Velocity Constraint} &&: V_{ex} = V_c\ \cos(\theta_1+\theta_2) = V_{sx} + A_x(T_2+T_3) + \frac{1}{2}J_{1x}T_1^2 - \frac{1}{2}J_{3x}T_3^2\\ &\text{Displacement Constraint:} && \varepsilon_x = V_c\ \cos(\theta_1)\left(T_1+\frac{T_2}{2}\right) + \frac{1}{2}A_x\left(\frac{T_2}{2}\right)^2 + \frac{1}{6}J_{1x}T_1^3 + \frac{1}{2}J_{1x}T_1^2\left(\frac{T_2}{2}\right) - V_c\ \cos(\theta_1)\left(T_1+\frac{T_2}{2}\right)\end{aligned}\right\} \tag{26}$$

and motion durations T_1, T_2 and T_3 are identified with respect to axis acceleration and jerk limits as follows.

Firstly, the algorithm assumes that a constant acceleration phase exists during cornering motion. This implies that the acceleration and jerk limits of X axis are fully exploited by setting $_{Ax}=A_{max}, J_{1x}=J_{max}=-J_{3x}$, and the duration of constant jerk phase, T_1 and T_3 are computed by the trapezoidal nature of JLAP as:

$$T_1 = T_3 = \frac{A_{\max}}{J_{\max}}. \tag{27}$$

Duration of the constant acceleration phase, T_2 is then obtained from Eq. (20):

$$T_2 = \frac{\Delta V_x}{A_{\max}} - \frac{A_{\max}}{J_{\max}}, \tag{28}$$

and the maximum cornering velocity, V_c is solved from displacement boundary condition given in Eq. (26) as:

$$V_c = \frac{\sqrt{8A_{\max}\,\varepsilon\left|\sin\left(\theta_1+\frac{\theta_2}{2}\right)\right| - \frac{{A_{\max}}^4}{3{J_{\max}}^2}}}{\left|\cos(\theta_1+\theta_2) - \cos(\theta_1)\right|} \tag{29}$$

On the other hand, if the velocity transition is small and acceleration capacity of the drives is large, T_2 computed from Eq. (28) may become negative $T_2<0$. In this case, constant acceleration phase becomes unnecessary, and it is eliminated by setting $T_2=0$. Eq. (26) is used to re-calculate maximum axis acceleration as

$$A_x = \sqrt[3]{6{J_{\max}}^2\ \varepsilon|\cos(\theta_\varepsilon)|}. \tag{30}$$

and the durations of constant jerk section, T_1 and T_3 are updated to:

$$T_1 = T_3 = \frac{A_x}{J_{\max}} \tag{31}$$

As a result, the fastest cornering velocity can be obtained from Eq. (26) as:

$$V_c = \frac{\sqrt[3]{36J_{\max}\ \varepsilon^2\sin^2\left(\theta_1+\frac{\theta_2}{2}\right)}}{\left|\cos(\theta_1+\theta_2) - \cos(\theta_1)\right|} \tag{32}$$

For some applications where feedrate is slow and the corner geometry is severely obtuse, cornering velocity V_c computed from Eqs. (29) or (32) may exceed the commanded feedrate. In this case, the cornering velocity is set to the programmed feedrate of the linear

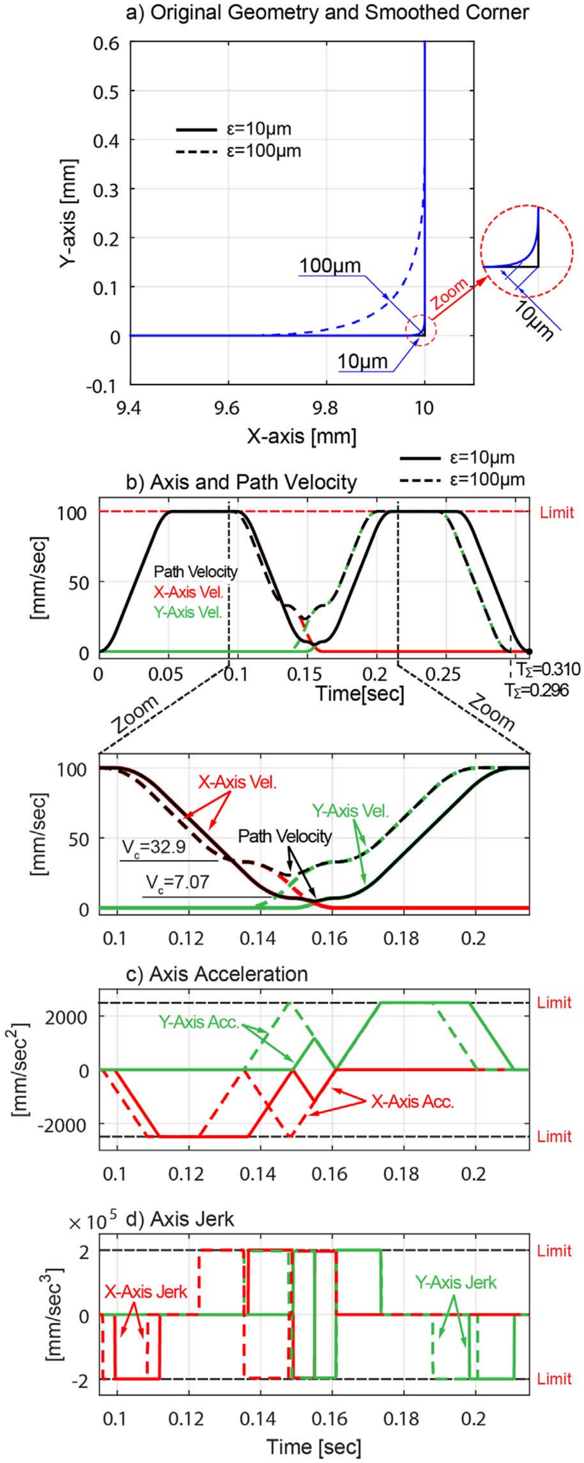

Fig. 5. Right-handed Sharp Corner Smoothing using KCS method with Interrupted acceleration.

segment. Cornering acceleration and jerk profiles are solved from Eq. (26) to satisfy the desired cornering tolerance. Please note that since cornering velocity is lowered, maximum acceleration and jerk limits of the drives may not be saturated leading to a near time-optimal cornering motion.

The total cornering duration is calculated by sum of all durations of the JLAP:

$$T_C = T_1 + T_2 + T_3 \tag{33}$$

On the other hand, if Y-axis experiences the largest velocity transition, then maximum cornering speed, V_c is computed by replacing cosine terms with sine in Eqs. (29) and (32). Please note that the JLAP for less demanding, so-called the "trailing", axis is planned with identical segment durations computed from Eqs. (27), (28) and (31). As a result, the trailing axis is not driven at its kinematic limits, but overall cornering motion is synchronized.

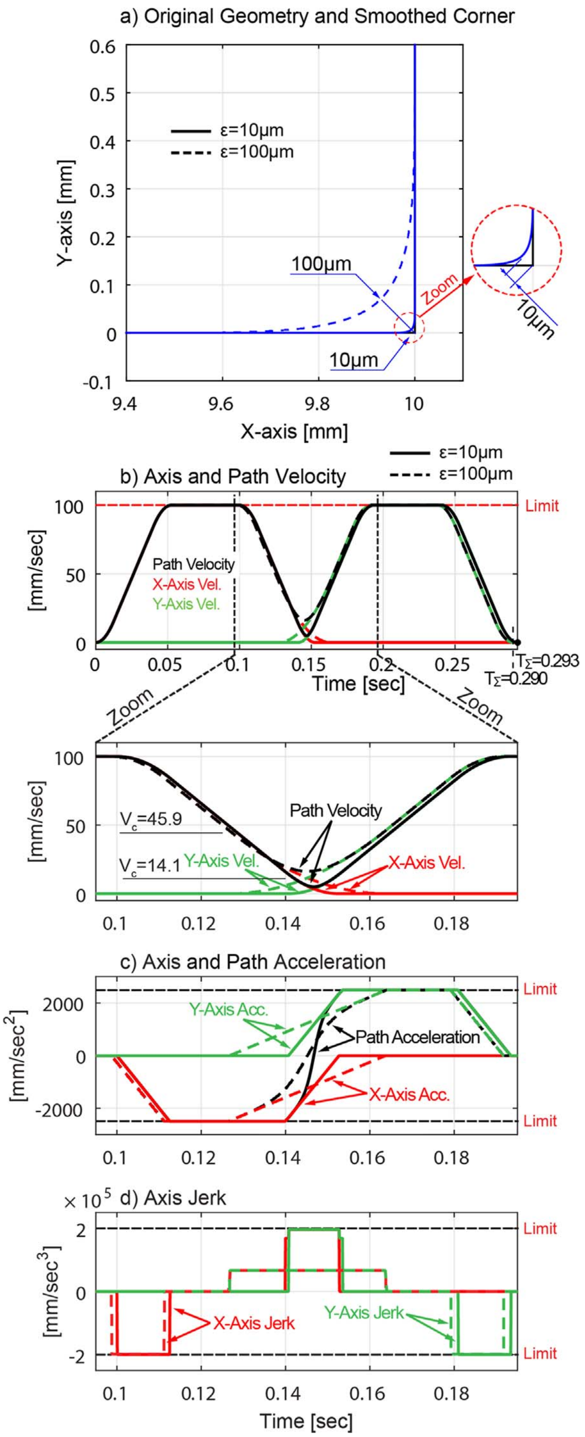

Fig. 6. Right-handed Sharp Corner Smoothing using KCS method with Uninterrupted acceleration.

2.3. *Kinematic corner smoothing (KCS) with uninterrupted acceleration*

Previous section presented the kinematic corner smoothing(KCS) approach based on blending constant axis velocities at the entry and exit of a cornering motion. In that algorithm tangential velocity is reduced to the fastest cornering V_c, and cornering motion starts and ends with zero initial acceleration (See Fig. 2b). In an effort to further reduce overall cornering duration, this section extends the approach presented in Section 2.2 by introducing cornering acceleration boundary conditions, A_c. The objective is to realize an uninterrupted tool motion as it is decelerated from segment's programmed feedrate to the cornering velocity and accelerated back to the next segment's feed without interrupting acceleration. Thus, the KCS with uninterrupted acceleration method presented in this section imposes non-zero cornering boundary acceleration conditions to further reduce overall cornering cycle time.

Fig. 4 presents the approach to blend both axis velocity and accelerations in an uninterrupted manner. Instead of employing all 3 phases of the JLAP as proposed in Section 2.2, only the acceleration ramp phase, i.e. phase 1, is employed to smoothly interpolate axis velocity and accelerations from start to the end of the corner. The cornering motion kinematics can be written for X and Y axes as:

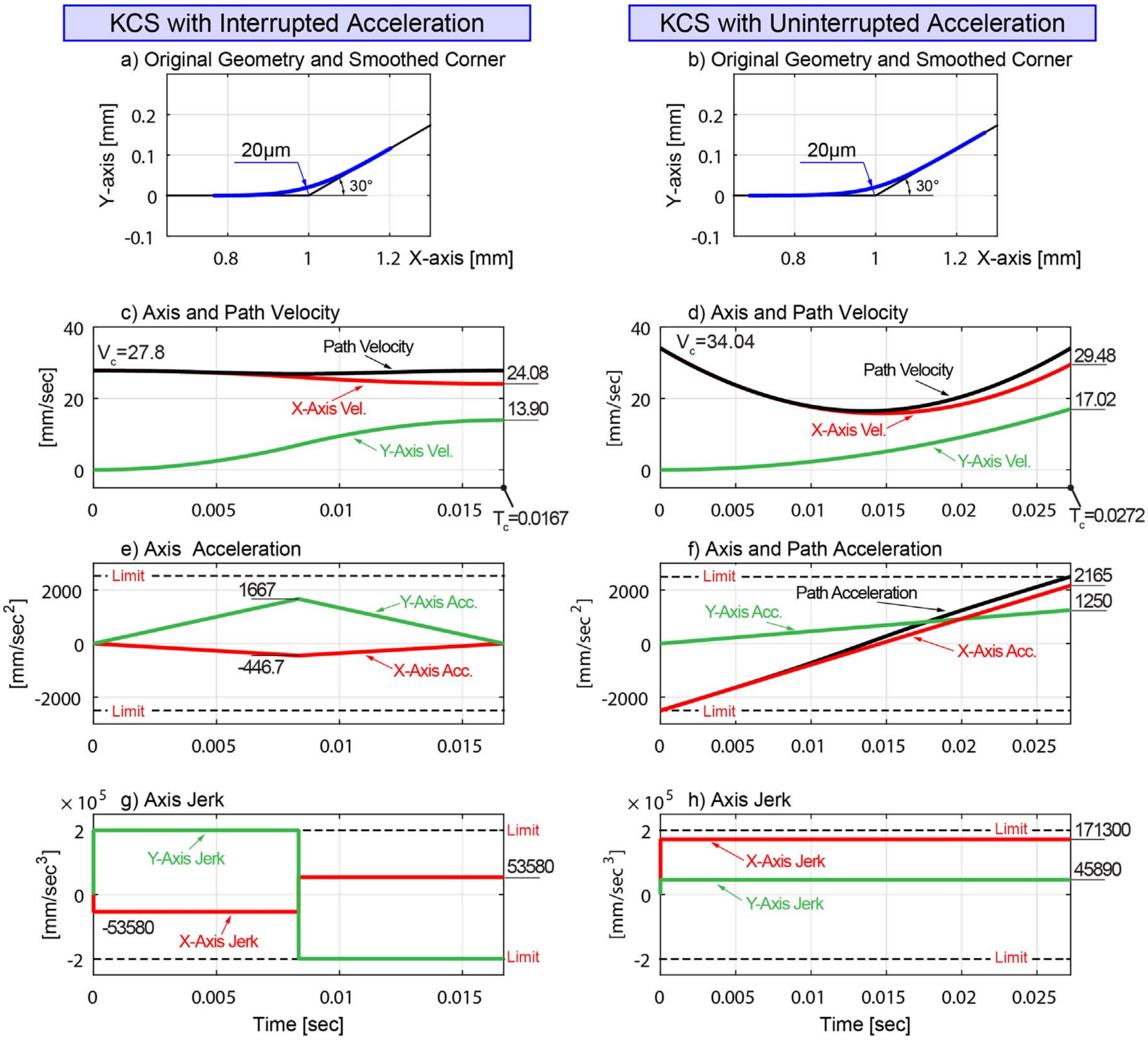

Fig. 7. Obtuse corner smoothing using KCS with interrupted and uninterrupted acceleration profiles.

$$\underbrace{\left\{\begin{aligned} j_x(\tau) &= J_x \\ a_x(\tau) &= A_{sx} + J_x\tau \\ v_x(\tau) &= V_{sx} + A_x\tau + \frac{1}{2}J_x\tau^2 \\ s_x(\tau) &= V_{sx}t + \frac{1}{2}A_x\tau^2 + \frac{1}{6}J_x\tau^3 \end{aligned}\right\}}_{X-axis} \text{ and } \underbrace{\left\{\begin{aligned} j_y(\tau) &= J_{1y} \\ a_y(\tau) &= A_{sy} + J_y\tau \\ v_y(\tau) &= V_{sy} + A_y\tau + \frac{1}{2}J_y\tau^2 \\ s_y(\tau) &= V_{sy}\tau + \frac{1}{2}A_y\tau^2 + \frac{1}{6}J_y\tau^3 \end{aligned}\right\}}_{Y-axis} \; 0 \le t \le t_1 \tag{34}$$

Firstly, identical tangential acceleration magnitudes at the start and end of the cornering motion $A_c = -A_s = A_e$, are imposed to generate a symmetric cornering trajectory,

$$\underbrace{\left\{\begin{aligned} A_{sx} &= -A_c\cos(\theta_1) \\ A_{sy} &= -A_c\sin(\theta_1) \end{aligned}\right\}}_{\text{Starting Acceleration Constraints}}, \underbrace{\left\{\begin{aligned} A_{ex} &= A_c\cos(\theta_1+\theta_2) = A_{sx} + J_xT_1 \\ A_{ey} &= A_c\sin(\theta_1+\theta_2) = A_{sy} + J_yT_1 \end{aligned}\right\}}_{\text{Ending Acceleration Constraints}} \tag{35}$$

Similarly, velocity boundary conditions are imposed as:

$$\underbrace{\left\{\begin{aligned} V_{sx} &= V_c\cos(\theta_1) \\ V_{sy} &= V_c\sin(\theta_1) \end{aligned}\right\}}_{\text{Starting Velocity Constraints}}, \underbrace{\left\{\begin{aligned} V_{ex} &= V_c\cos(\theta_1+\theta_2) = V_{sx} + A_{sx}T_1 + 1/2J_xT_1^2 \\ V_{ey} &= V_c\cos(\theta_1+\theta_2) = V_{sy} + A_{sy}T_1 + 1/2J_yT_1^2 \end{aligned}\right\}}_{\text{Ending Acceleration Constraints}} \tag{36}$$

Lastly, displacement boundary conditions are introduced. Planning cornering motion with identical start and ending tangential velocity and accelerations ensures that the trajectory is symmetric around the bisector of the corner, hence maximum cornering error occurs at the mid-point of the trajectory. The mid-point position can be computed from Eq. (34) as

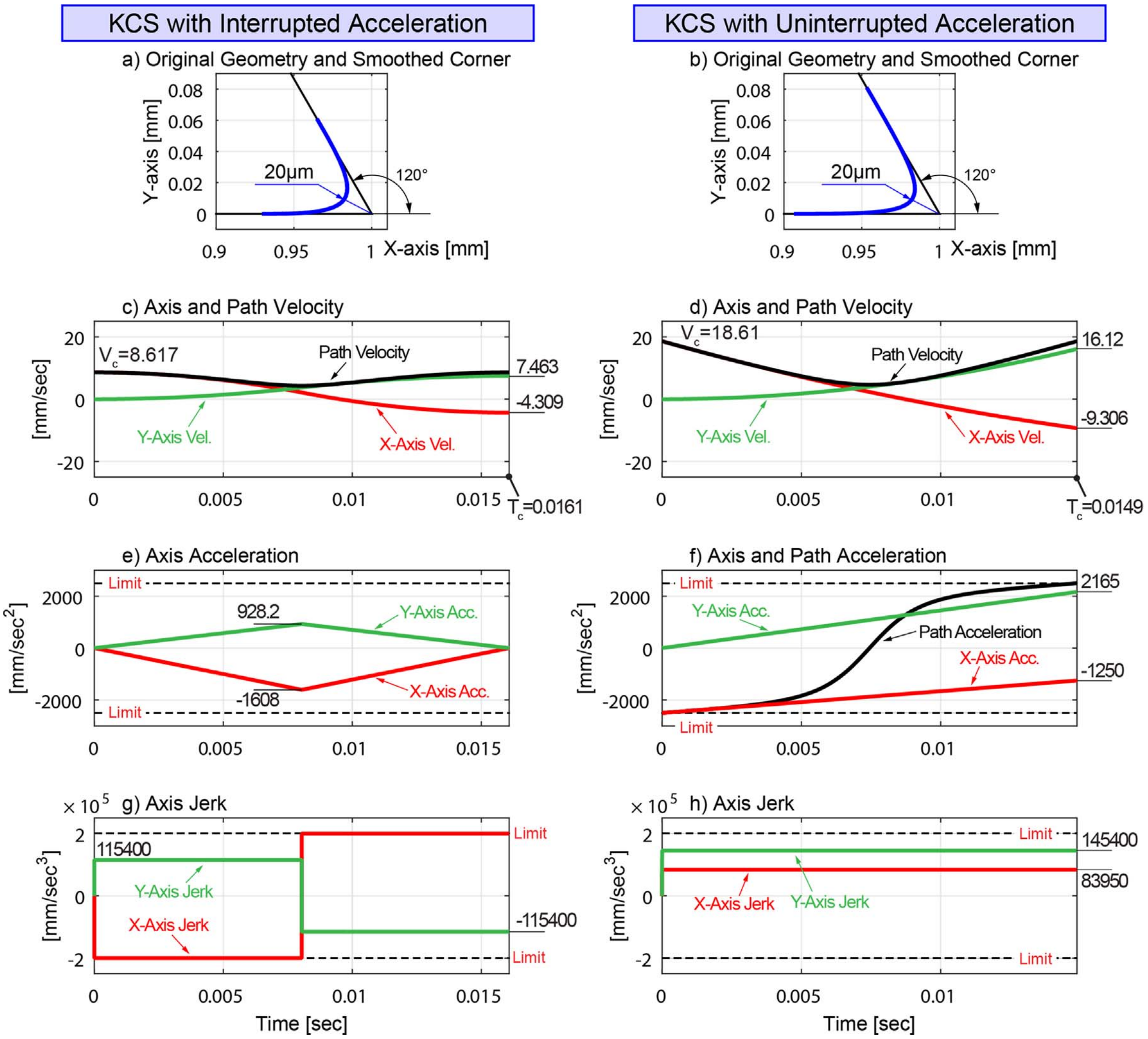

Fig. 8. Acute corner smoothing based on KCS with interrupted and uninterrupted acceleration profiles.

$$\left.\begin{aligned} x_{mid} &= V_{sx}\frac{T_1}{2} + \frac{1}{2}A_{sx}\left(\frac{T_1}{2}\right)^2 + \frac{1}{6}J_x\left(\frac{T_1}{2}\right)^3 \\ y_{mid} &= V_{sy}\frac{T_1}{2} + \frac{1}{2}A_{sy}\left(\frac{T_1}{2}\right)^2 + \frac{1}{6}J_y\left(\frac{T_1}{2}\right)^3 \end{aligned}\right\}, \tag{37}$$

and location of the sharp corner point is computed from cornering geometry (See Fig. 4a) as:

$$P_c = \begin{cases} x_c = L_c \ \cos(\theta_1) \\ y_c = L_c \ \sin(\theta_1) \end{cases} \tag{38}$$

where L_c is calculated based on the distance x-axis traveled from Eq. (34):

$$L_c = \left| \frac{V_{sx}T_1 + \frac{1}{2}A_{sx}T_1^2 + \frac{1}{6}J_x T_1^3}{\cos(\theta_1) + \ \cos(\theta_1 + \theta_2)} \right| \tag{39}$$

The displacement boundary condition for cornering trajectory is imposed to control cornering tolerance from Eqs. (38) and (37). For the X-axis it can be written as:

$$\varepsilon_x = x_{mid} - x_c = \varepsilon \ \cos(\theta_\varepsilon) = \frac{\left\{ \begin{aligned} & V_{sx}T_1\tfrac{1}{2}\left(\cos(\theta_1+\theta_2) - \ \cos(\theta_1)\right) + \tfrac{1}{2}A_{sx}T_1^2\left(\tfrac{1}{4}\ \cos(\theta_1+\theta_2) - \tfrac{3}{4}\ \cos(\theta_1)\right) \\ & + \tfrac{1}{6}J_x T_1^3\left(\tfrac{1}{8}\ \cos(\theta_1+\theta_2) - \tfrac{7}{8}\ \cos(\theta_1)\right) \end{aligned} \right\}}{\cos(\theta_1) + \ \cos(\theta_1+\theta_2)} \tag{40}$$

Please note that Y-axis component is simply obtained by replacing cosine terms with sine and axis acceleration and jerk amplitudes. Similar to Section 2.2, maximum cornering velocity, V_c is sought to generate the fastest cornering speed, which tries to saturate at least

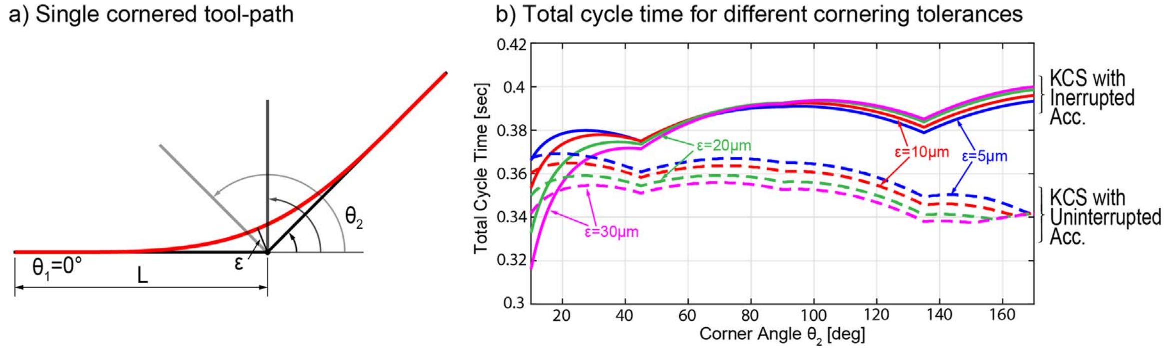

Fig. 9. Cycle time performance of KCS with interrupted and uninterrupted acceleration profiles.

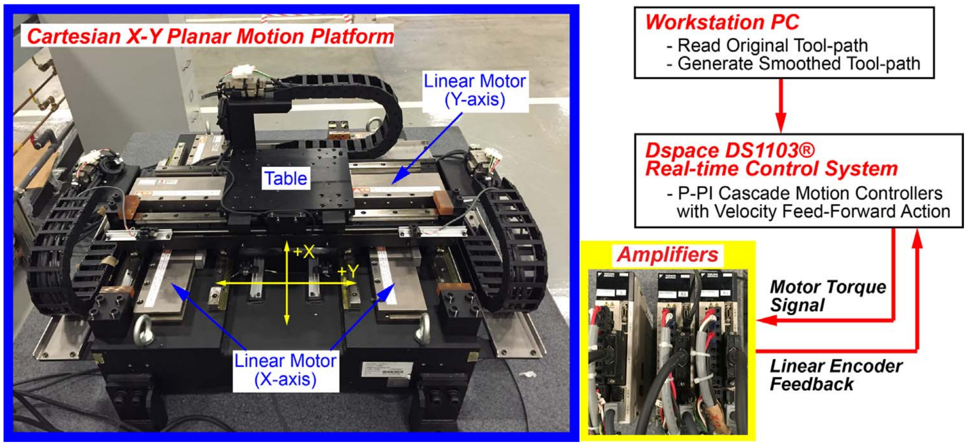
Cartesian X-Y Planar Motion Platform
Linear Motor (Y-axis)
Table
+X
+Y
Linear Motor (X-axis)
Workstation PC
- Read Original Tool-path
- Generate Smoothed Tool-path
Dspace DS1103®
Real-time Control System
- P-PI Cascade Motion Controllers with Velocity Feed-Forward Action
Amplifiers
Motor Torque Signal
Linear Encoder Feedback

Fig. 10. Experimental setup.

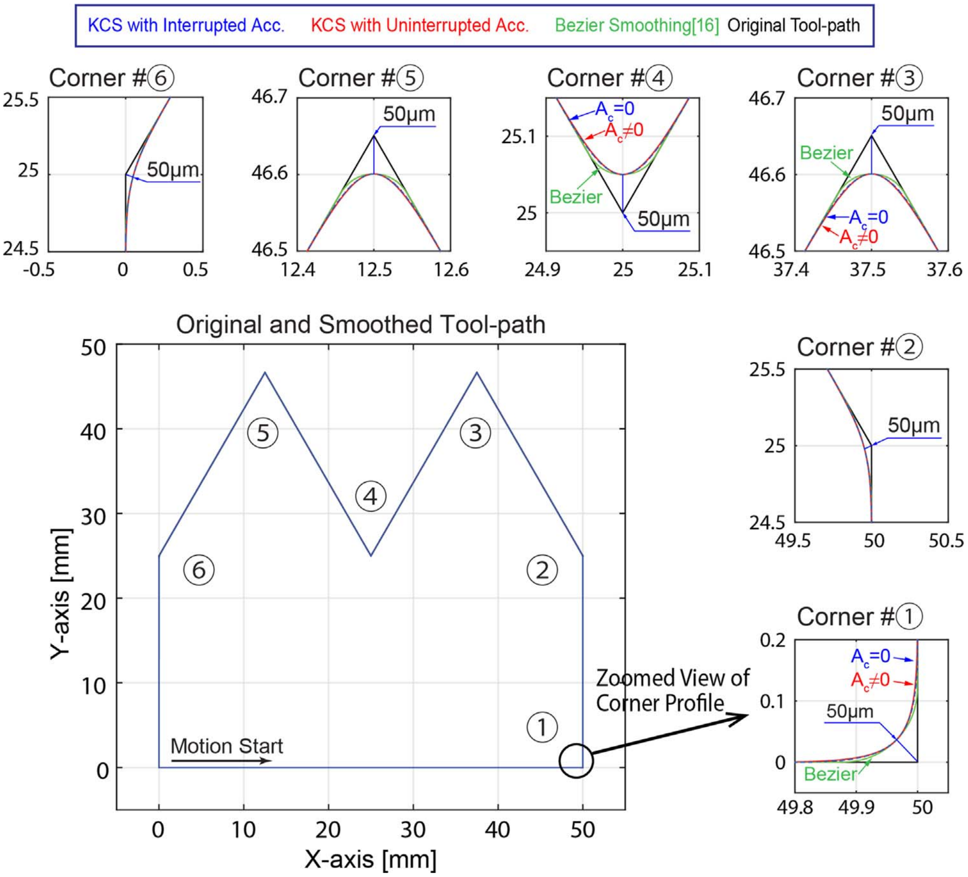

Fig. 11. Experimental multi-segmented tool-path.

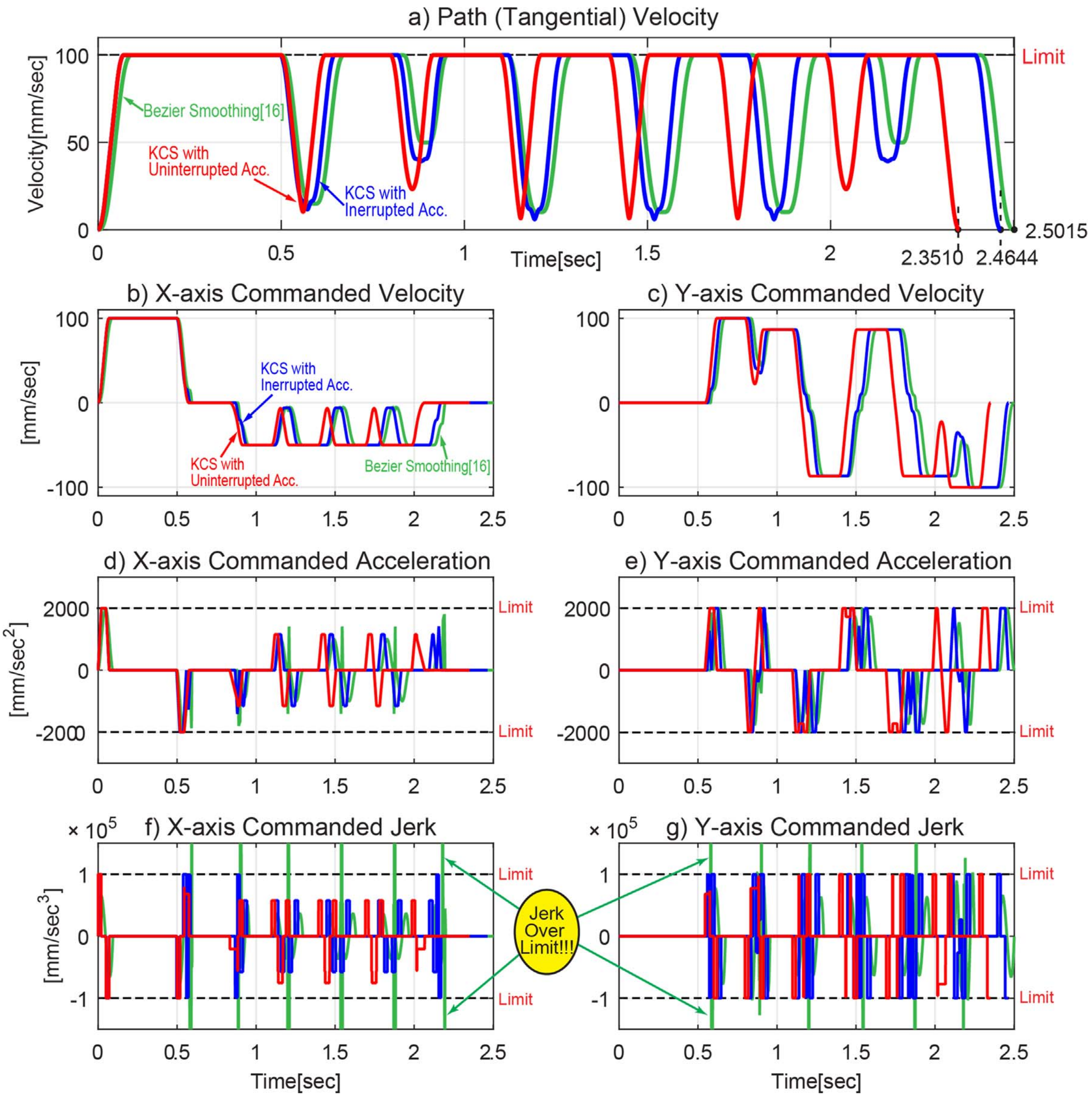

Fig. 12. Kinematic profiles along corner smoothened tool-path.

one of the axis' acceleration or jerk limits. The limiting axis is identified as the axis with the largest acceleration transition $\Delta A_x = |A_{ex} - A_{sx}|$ or $\Delta A_y = |A_{ey} - A_{sy}|$. For instance, identifying X-axis as the limiting axis, $\Delta A_x > \Delta A_y$, acceleration, velocity and position constraints for cornering motion are written from Eqs. (35), (36) and (40) as:

$$\left.\begin{array}{l}
\text{Acc. Constraint}\ :\ A_c\ \cos(\theta_1+\theta_2) = \ -A_c\ \cos(\theta_1) + J_x T_1 \\
\text{Vel. Constraint}\ :\ V_c\ \cos(\theta_1+\theta_2) = V_c\ \cos(\theta_1) - A_c\ \cos(\theta_1)T_1 + \dfrac{1}{2}J_x T_1^2 \\
\text{Disp. Constraint}:\ \varepsilon\ \cos\left(\dfrac{\pi}{2}+\theta_1+\dfrac{\theta_2}{2}\right) = V_c\ \cos(\theta_1)\left(\dfrac{T_1}{2}\right) - \dfrac{1}{2}A_c\ \cos(\theta_1)\left(\dfrac{T_1}{2}\right)^2 + \dfrac{1}{6}J_x\left(\dfrac{T_1}{2}\right)^3 \\
\qquad\qquad - \left(\dfrac{V_c\ \cos(\theta_1)T_1 - \frac{1}{2}A_c\ \cos(\theta_1)T_1^2 + \frac{1}{6}J_x T_1^3}{\cos(\theta_1) +\ \cos(\theta_1+\theta_2)}\right)\cos(\theta_1)
\end{array}\right\} \tag{41}$$

Feasible cornering velocity trajectory is then sought by saturating either one of the kinematic limits. For instance, setting cornering jerk, J_x=J_{max} allows computation of the unknown cornering velocity, V_c as

$$V_{c,J\ \max} = 2\sqrt[3]{\left|\frac{9\varepsilon^2 J_{\max}}{\sin^2\left(\frac{\theta_2}{2}\right)\left(\cos(\theta_1) +\ \cos(\theta_1+\theta_2)\right)}\right|} \tag{42}$$

Similarly, the fastest cornering velocity that saturates acceleration limit of the axis is computed by setting ${}_{Ax}$=A_{max}:

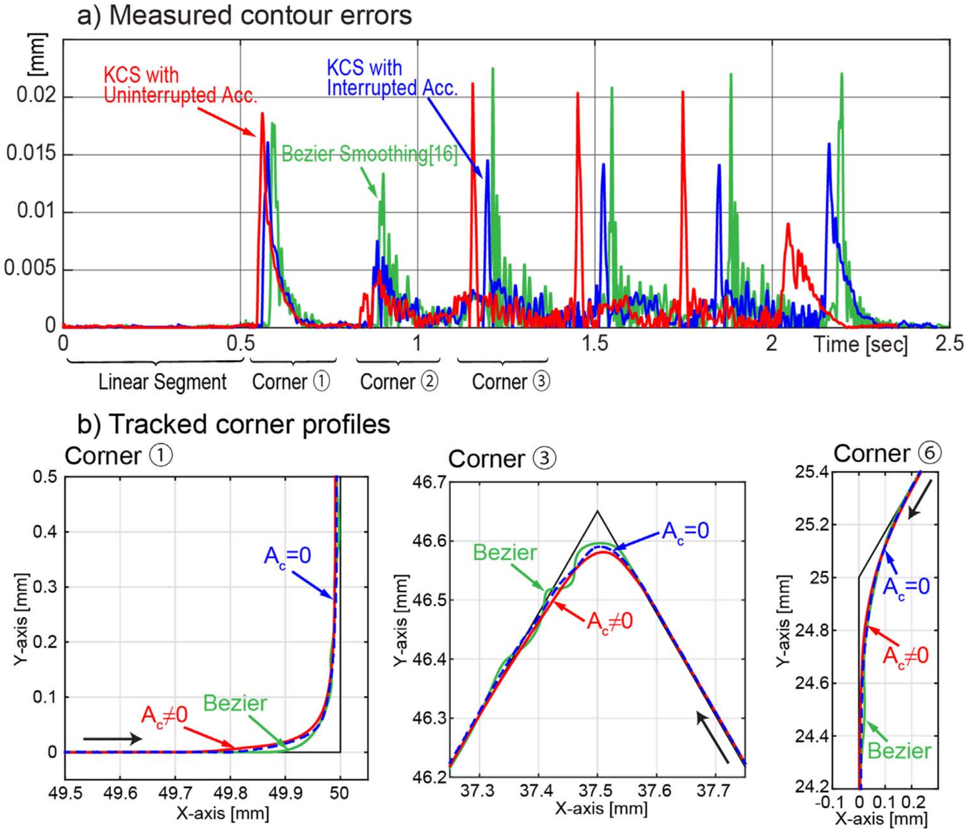

Fig. 13. Experimentally recorded contouring performance.

Table 1
Cycle time and contouring performance comparison.

Algorithms	Cycle time [s]	Contour error	
		RMS [μm]	Max [μm]
KCS with uninterrupted Acc. (proposed)	2.3510	3.0637	21.2576
KCS with interrupted Acc. (proposed)	2.4644	2.8062	16.1245
Bezier smoothing ([16])	2.5015	3.1517	22.5685

$$V_{c,A\ \max} = \sqrt{\left|\frac{6A_{\max}\,\varepsilon}{\sin\left(\frac{\theta_2}{2}\right)}\right|} \qquad (43)$$

In order to satisfy both kinematic limits, V_c is selected from Eqs. (42) and (43) as:

$$V_c = \min\left\{V_{c,J\ \max}, V_{c,A\ \max}\right\} \qquad (44)$$

The cornering acceleration is then computed from Eq. (43). Finally, duration of the cornering motion is solved from Eq. (41):

$$T_1 = \frac{12\varepsilon}{V_c\ \sin\left(\frac{\theta_2}{2}\right)} \qquad (45)$$

Based on the cornering velocity and acceleration, fastest cornering motion duration is computed, which saturates kinematic limits one of the drives. The “trailing” axis motion is planned for identical cornering duration T_1 to ensure that the motion is synchronized. The trailing axis' acceleration and jerk amplitudes, J_y and A_y are computed by re-writing Eq. (41), accordingly.

Please note that in case if the cornering velocity computed from Eq. (44) exceeds programmed feedrate of the linear block, it is lowered and set to the linear segment's feedrate. The acceleration and jerk amplitudes are computed from Eq. (41), and the motion is re-planned.

3. Illustrative examples and experimental validation

This section evaluates performance of the proposed kinematic corner blending techniques on various high-speed cornering case scenarios. Experimental results and benchmarks to widely used geometric corner smoothing technique are also presented to validate effectiveness of the proposed cornering smoothing method.

3.1. Illustrative examples

Firstly, Fig. 5 and Fig. 6 show application of the proposed corner smoothing techniques on a right-handed sharp corner, i.e. $\theta_1 = 0°$, and $\theta_2 = 90°$ with two different, 10[μm] and 100[μm], cornering tolerances. The acceleration and jerk limitations of the drives (X and Y axes) are set to A_{max}=2.5×10^3[mm/sec^2] and J_{max}=2×10^5[mm/sec^3]. Fig. 2 illustrated the kinematic corner smoothing (KCS) with interrupted acceleration presented in Section 2.2. Fig. 5a shows smoothened cornering geometry with ε=100[μm] and ε=10[μm] cornering tolerances. Fig. 5b shows generated axis and path velocity profiles. As shown, when approached to the corner, tangential velocity is reduced from the programmed feedrate of 100[mm/sec] to the specified cornering velocity. Depending on the cornering tolerance, the fastest cornering velocity is computed from Eqs. (29) or (32). For large contouring error, ε=100[μm], the resultant cornering velocity is V_c=32.9[mm/sec], and total motion time to finish the path is T_Σ=0.296[sec]. In contrast, tighter corner tolerance dictates slower cornering speed. When ε=10[μm] cornering velocity is calculated as V_c=7.07[mm/sec], and resulting cycle time is T_Σ=0.310[sec]. Notice from axis motion profiles, when approached to a right hand corner, X-axis simply decelerates to a full stop and Y-axis starts accelerating. The timing of this deceleration/acceleration transition determines the cornering tolerance. Both drives use their full acceleration and/or jerk limits. Particularly, if cornering error is large, acceleration limits of the drives can be saturated. This delivers a faster cornering motion. When cornering tolerance is small, the acceleration limits of the drives cannot be saturated within the allowed jerk bounds.

Fig. 6, on the other hand, presents results of the kinematic corner smoothing (KCS) algorithm with uninterrupted acceleration presented in Section 2.3. As observed from Fig. 6b, cornering motion has non-zero acceleration at the start and end. Maximum cornering velocities are computed to be V_c=45.9 and V_c=14.1, for ε=100[μm] and ε=10[μm], respectively. The resultant total cycle times are T_Σ=0.290[sec] and T_Σ=0.293[sec]. Although, KCS with uninterrupted acceleration requires more time during cornering motion, the total cycle time to travel the tool-path is slightly faster. As shown in Fig. 6c–d, drives decelerate at maximum rate to the corner in an effort to reduce the cycle time. Therefore, the cornering entry and exit acceleration are saturated, i.e. A_c=A_{max}=2500[mm/sec^2]. As shown in Fig. 6d, if cornering tolerance is small, this requires maximum jerk to be utilized to finish the cornering trajectory. However, if the cornering tolerance is large, the motion does not need to utilize full jerk capability to alter its acceleration and velocity. Thus, setting cornering error to ε=100[μm] (See Fig. 6d) only saturates acceleration limits of the drives but does not fully exploit jerk limits, which makes the KCS with uninterrupted acceleration near-time optimal. Fig. 9 shows a cycle time comparison between KCS algorithms with interrupted and uninterrupted acceleration profiles.

Fig. 7 and Fig. 8 show kinematic corner smoothing applied to *obtuse* and *acute* corners. In both cases cornering tolerance is set to ε=20 [μm]. Proposed algorithms with interrupted and uninterrupted accelerations can smoothen corners within given cornering tolerance. In case of the acute corner, resultant cornering velocities are much smaller. This is simply due to fact that X-axis must alter it motion direction, and has to undergo larger velocity traverse. In the obtuse case, Y-axis undergoes similar amount of velocity transition but does not change its motion direction. Notice that since total velocity traverses are similar, total cornering cycle times are actually comparable.

Next, cycle time performance of the KCS with interrupted and uninterrupted acceleration techniques is compared in Fig. 9. A single corner is smoothened by two L=10[mm] long linear segments. The desired feedrate along the tool-path is set to 100[mm/sec]. As shown in Fig. 9a, cornering angle is altered from acute to obtuse to compare the performance of KCS algorithms for different cornering geometries. Fig. 9b shows total cycle time for different cornering tolerances. As noticed, for very obtuse corners, i.e. cornering angle $\theta_2 < 20$, the KCS algorithm with interrupted acceleration delivers faster cycle time. In contrast, as the corner gets acute the un-interrupted acceleration provides faster cycle times. This can be attributed to the fact that as the corner gets sharper, cornering velocity becomes smaller. In this case, KCS with uninterrupted acceleration can plan efficient acceleration profiles and minimize the cycle time. Combination of the KCS algorithms with and without uninterrupted acceleration should be used to attain the fastest cycle time.

3.2. Experimental results

Lastly, experimental validation and benchmark comparisons are performed. The experimental Cartesian X–Y motion system is shown in Fig. 10. The planar motion table is driven by 3 linear motors. The heavier X-axis is designed as gantry and carries the lighter Y-axis. In order to implement proposed algorithms servo amplifiers are set to operate in torque (current) control mode. Closed loop control is implemented in the Dspace DS1103® real time control system by reading linear encoder feedback at a resolution of 0.7125[μm] and commanding torque signal to the servos at a closed loop sampling interval of T_s= 0.1[msec]. Both X and Y drives are controlled by P–PI cascade [29] motion controllers with velocity feed-forward action. The position feedback control bandwidths of the axes are roughly matched at $\omega_n = 35[Hz]$ to ensure good motion synchronization and path tracking.

3 algorithms are implemented and compared to each other on smoothing the tool-path shown in Fig. 11. Proposed KCS algorithms with interrupted and uninterrupted accelerations are implemented separately. They are compared against a geometric corner smoothing algorithm by Sencer et.al. [16], which fits curvature optimal Beziers around sharp corners and plans jerk limited feedrate profile for minimum cycle time. This method is called as the “Bezier” method. All the algorithms are computed off-line, sampled and commanded in real-time to the motion controllers. Reference motion commands are discretized by rounding the motion durations so that number of samples is integer while keeping the total displacement unchanged.

Fig. 11 shows smoothened tool-path clearly. The cornering error is set to ε=50[micron] for all the corners, and all the algorithms successfully smooth corners within given tolerance. Fig. 12 depicts motion profiles along the tool-path. The feedrate is set to f=100[mm/sec], axis acceleration and jerk limits are set to A_{max}=2×10^3,J_{max}=1×10^5. Fig. 12a shows tangential velocity profiles. As shown, proposed KCS technique with uninterrupted acceleration achieves the fastest cycle time amongst all the other methods. This is mainly due to the fact that most corners are acute. Acceleration and jerk profiles for all the methods are compared in Fig. 12d–g. As shown, all the methods respect acceleration limits of the drives. The Bezier corner-smoothing method fits a curvature optimal Bezier around the corner and selects the fastest cornering speed with respect to acceleration limits of the drives. Therefore, it is able to saturate acceleration limits of drives, but cannot respect jerk limits. As a matter of fact, if the algorithm is modified to utilize jerk bounds cornering velocity must be reduced greatly. In contrary, the proposed KCS algorithms clearly respect jerk limits of the drives (See Fig. 12f–g). As will be observed in the contouring errors, this functionality allows generation of a traceable smoother motion.

It is known that jerk content of the trajectory affects tracking errors and vibratory behavior of feed drive system [30]. Fig. 13 shows experimentally measured contouring errors along the corner smoothened tool-path. Since the *X* and *Y*-axis closed loop bandwidths are matched, contour errors along linear segments are negligible. Largest contouring errors occur at the cornering sections where static friction impacts drives, and acceleration and jerk profiles show large changes when drives alter their motion direction. Table 1 summarizes contouring performance of cornering algorithms and overall contour performances. Proposed KCS algorithms and Bezier corner smoothing method deliver similar overall contouring performances. To be exact, proposed KCS methods deliver slightly better RMS and maximum contour errors. The KCS with interrupted acceleration can provide ~20% reduction in maximum contour errors while staying within acceleration and jerk limits of the drives and still deliver faster cycle times. Furthermore, if error profiles are inspected closely Bezier method [16] shows severe error fluctuations around the cornering durations. This is simply due to extremely high jerk amplitude commanded to the drives. Since jerk is not limited to a suitable level, large jerk spikes excite the feedback control system and induce vibrations. These vibrations are visible on the actual trajectory. As noted from Fig. 13, resultant tool-path fluctuates severally around the cornering sections. These fluctuations will be imprinted on the part surface during an actual manufacturing operation and destroy process tolerances. Proposed technique can limit the jerk and provide a smoother motion with faster cycle time. As noted from Table 1, proposed KCS method with uninterrupted acceleration can reduce cycle time around 6–7% for this simple tool-path. For a longer tool-path, which consists large number of corners the effect would be much more pronounced.

4. Conclusions

This paper proposes novel kinematic corner smoothing(KCS) techniques, which eliminate the need for two-step geometry based corner rounding methods. The proposed algorithms blend axis velocities around sharp corners with jerk limited acceleration transitions and generate symmetric rounded corner profiles with precisely controlled geometric tolerances. The cornering duration is calculated based on the cornering tolerance, axis kinematic limits and sharp corner profile to minimize overall cycle time. Proposed algorithm is fully analytical and provides fast and efficient real-time implementation on 2 to 3 axis Cartesian CNC machine tools. Extensive illustrative examples along obtuse and acute corner profiles validate accuracy and performance of the proposed algorithms. Experimental benchmarks against spline based corner smoothing technique show that proposed algorithms provide better contouring performance while reducing overall cycle time 6–7% for a tool-path with six corners. Considering that longer tool-paths, such as the ones used in high speed die and mold manufacturing, may contain hundred and thousands of sharp corners, proposed techniques provide significant potential to reduce overall cycle times.

References

[1] L. Piegl, W. Tiller, The NURBS Book, 2nd (ed.), Springer-Verlag, Berlin Heidelberg, 2003.
[2] Y. Koren, R.-S. Lin, Five-axis surface interpolators, Ann. CIRP 44 (1) (1995) 379–382.
[3] Q.G. Zhang, R.B. Greenway, Development and implementation of a NURBS curve motion interpolator, Robot. Comput. Integr. Manuf. 14 (1) (1998) 27–36.
[4] J.M. Langeron, E. Duc, C. Lartigue, P. Bourdet, A new format for 5-axis tool path computation using Bspline curves, Comput. Aided Des. 36 (12) (2004) 1219–1229.
[5] F.-C. Wang, P.K. Wright, B.A. Barsky, D.C.H. Yang, Approximately arc-length parameterized C3 quintic interpolatory splines, ASME J. Mech. Des. 121 (3) (1999) 430–439.
[6] S. Timar, R. Farouki, T. Smith, C. Boyadjieff, Algorithms for time-optimal control of CNC machines along curved tool paths, Robot. Comput. Integr. Manuf. 21 (2005) 37–53.
[7] M. Heng, K. Erkorkmaz, Design of a NURBS interpolator with minimal feed fluctuation and continuous feed modulation capability, Int. J. Mach. Tools Manuf. 50 (2010) 281–293.
[8] K. Erkorkmaz, Y. Altintas, Quintic spline interpolation with minimal feed fluctuation, ASME J. Manuf. Sci. Eng. 127 (2) (2005) 339–349.
[9] K. Erkorkmaz, C.H. Yeung, Y. Altintas, Virtual CNC system. Part II. High speed contouring application, Int. J. Mach. Tools Manuf. 46 (10) (2006) 1124–1138.
[10] M.K. Jouaneh, Z. Wang, D.A. Dornfeld, Trajectory planning for coordinated motion of a robot and a positioning table. Part 1. Path specification, IEEE Trans. Robot. Autom. 6 (1990) 735–745.
[11] M.K. Jouaneh, D.A. Dornfeld, M. Tomizuka, Trajectory planning for coordinated motion of a robot and a positioning table. Part 2. Optimal trajectory specification, IEEE Trans. Robot. Autom. 6 (1990) 746–759.
[12] C. Ernesto, R. Farouki, High-speed cornering by CNC machines under prescribed bounds on axis accelerations and toolpath contour error, Int. J. Adv. Manuf. Technol. 58 (2012) 327–338.
[13] S. Tulsyan, Y. Altintas, Local toolpath smoothing for five-axis machine tools, Int. J. Mach. Tools Manuf. 96 (2015) 15–26.
[14] M. Duan, C. Okwudire, Minimum-time cornering for CNC machines using an optimal control method with NURBS parameterization, Int. J. Adv. Manuf. Technol. (2015) 1–14.
[15] S.J. Yutkowitz, W. Chester, Apparatus and Method for Smooth Cornering in a Motion Control System, United States, Siemens Energy & Automation, Inc., Alpharetta, GA, 2005, US Patent 6922606.
[16] B. Sencer, K. Ishizaki, E. Shamoto, A curvature optimal sharp corner smoothing algorithm for high-speed feed motion generation of NC systems along linear tool paths, Int. J. Adv. Manuf. Technol. 76 (9–12) (2015) 1977–1992.
[17] H. Zhao, L. Zhu, H. Ding, A real-time look-ahead interpolation methodology with curvature-continuous B-spline transition scheme for CNC machining of short line segments, Int. J Mach. Tools Manuf. 65 (2013) 88–98.
[18] V. Pateloup, E. Duc, P. Ray, B-spline approximation of circle arc and straight line for pocket machining, Comput. Aided Des. 42 (2010) 817–827.
[19] L. Zhang, Y. You, J. He, X. Yang, The transition algorithm based on parametric spline curve for high-speed machining of continuous short line segments, Int. J. Adv. Manuf. Technol. 52 (2011) 245–254.
[20] H. Zhao, Li-Min Zhu, H. Ding, A real-time look-ahead interpolation methodology with curvature-continuous B-spline transition scheme for CNC machining of short line segments, Int. J. Mach. Tools Manuf. 65 (2013) 88–98.
[21] Q. Bi, Y. Wang, L. Zhu, H. Ding, A practical continuous-curvature Bezier transition algorithm for high-speed machining of linear tool path, Intell. Robot. Appl. (2011) 465–476.
[22] X. Beudaert, S. Lavernhe, C. Tournier, 5-axis local corner rounding of linear tool path discontinuities, Int. J. Mach. Tools Manuf. 73 (2013) 9–16, http://dx.doi.org/10.1016/j.ijmachtools.2013.05.008.
[23] K. Erkorkmaz, Y. Altintas, High speed CNC system design. Part I: jerk limited trajectory generation and quintic spline interpolation, Int. J. Mach. Tools Manuf. 41 (9) (2001) 1323–1345.
[24] M.T. Lin, M.S. Tsai, H.T. Yau, Development of a dynamics-based NURBS interpolator with real-time look-ahead algorithm, Int. J. Mach. Tools Manuf. 47 (15) (2007) 2246–2262.
[25] Y. Altintas, K. Erkorkmaz, Feedrate optimization for spline interpolation in high speed machine tools, CIRP Ann. 52 (2003) 297–302.
[26] M. Weck, G. Ye, Sharp corner tracking using the IKF control strategy, CIRP Ann. Manuf. Technol. 39 (1) (1990) 437–441.

[27] B. Sencer, K. Ishizaki, E. Shamoto, High speed cornering strategy with confined contour error and vibration suppression for CNC machine tools, CIRP Ann. Manuf. Technol. 64 (1) (2015) 369–372.

[28] M.S. Tsai, Y.C. Huang, A novel integrated dynamic acceleration/deceleration interpolation algorithm for a CNC controller, Int. J. Adv. Manuf. Technol. (2016) 1–14.

[29] S.S. Yeh, P.L. Hsu, Perfectly matched feedback control and its integrated design for multiaxis motion systems, J. Dyn. Syst. Meas. Control. 126 (3) (2004) 547–557.

[30] P.J. Barre, R. Bearee, P. Borne, E. Dumetz, Influence of a jerk controlled movement law on the vibratory behaviour of high-dynamics systems, J. Intell. Robot. Syst. 42 (3) (2005) 275–293.